Received: October 18, 2023. Revised: December 11, 2023. 845

International Journal of
Intelligent Engineering & Systems

http://www.inass.org/

Single Feed, Compact Size, Wideband Circular Polarization Antenna Based on Inverted U-shape Parasitic Stub for ISM Band Applications

Alaa Imran Al-Muttairi[1]* Mohammed Jabbar Mohammed Ameen[2]
Ali Khalid Jassim[3]

[1]*Department of Biomedical Engineering, University of Babylon, Iraq*
[2] *Department of Electrical Engineering, University of Babylon, Babylon, Iraq*
[3]*Department of Electrical Engineering, University of Mustansiriyah, Baghdad, Iraq*
* Corresponding author's Email: al_al_44@uobabylon.edu.iq

Abstract: A new single feed, compact size, and wideband circular polarization (CP) antenna is designed in this work. The designed antenna is made of two layers of the commercially available FR-4 substrate. The geometry in this design consists of a proximity-coupled feeding line for excitation and a circular patch with peripheral cutes as a driven patch surrounded by an inverted U-shape stub as a parasitic patch. According to the design idea, every driven and parasitic patch would produce its own CP radiation. Therefore, the antenna's axial ratio bandwidth is expanded by creating two neighboring axial ratio (AR) minima points. An analysis study based on surface current and electrical field distributions is carried out to demonstrate the antenna's operation. The designed antenna is fabricated and measured. Results show that the reflection coefficient bandwidth is (8.5%), starting from (2.33GHz) to (2.55GHz), and the axial ratio bandwidth is (4.5%) starting from (2.42GHz) to (2.53GHz). The obtained co-pol/x-pol ratio is better than 13dB in the antenna broadside and the measured gain is around 4.8 dB over the entire required band. Based on the achieved results, the antenna is a good solution for ISM band applications and MIMO arrays.

Keywords: Wideband circular polarization antenna , Axial ratio bandwidth enhancement , U-shape parastic patch.

1. Introduction

In modern communication, circular polarization (CP) microstrip antennas (CPMA) are commonly used in different wireless systems due to their good propagation and size reduction features. In comparison to the linear polarization (LP) microstrip antenna, the CP antenna increases the reliability and the quality of the communication link by mitigating several channel issues such as multi-path interference, Faraday rotation, and antenna's orientation between transmitter and receiver especially for a mobile scenario [1, 2]. Typically, CPMA can be designed by exciting two orthogonal modes in phase quadrature to produce two different polarization senses: left-hand or right-hand CP [3]. Practically, CPMA is classified into two main categories namely: dual-feed or single-feed CP antenna[4]. The first type has a complex structure because it needs an external polarizer feeding network. On the contrary, a single-feed CP antenna has the simplest structure because it depends on perturbation segments to introduce little asymmetry in the geometry of the patch. Different perturbation methods are used such as slot or slits as in [5-8], corner truncating as in [9-11], peripherals cut as in [5], and stubs as in [12, 13]. All these methods work on producing two orthogonal and degenerated modes with equal amplitudes and out of phase by 90^o. Unfortunately, single-feed CPMAs suffer from an inherent narrow axial ratio band width (ARBW) which limits their applications (around 1.5%). Therefore, bandwidth enhancement techniques may be used to enable these antennas to work in modern high-speed communication systems.

Several methods are proposed in the open literature to enhance ARBW. Among them, adding parasitic elements vertically or horizontally in relation to the main radiator is the most interesting

and effective one. In [14], a wearable CP microstrip antenna is designed for body area network applications. The axial ratio (AR) bandwidth is improved by adding two inverted L-shape parasitic elements. The obtained ARBW reached to 3.85%. Good results are obtained with increasing antenna complexity. In [15], the ARBW of the traditional circular patch antenna is enhanced by inserting two annular sector shapes. The obtained bandwidth was equal to 3.3% but the size of the antenna increased significantly. In [16], a resonant parasitic patch (NFRP) is used to improve ARBW with a low profile. The presence of this patch beneath the main radiator introduces a new pair of orthogonal degenerated resonant modes which produce wider CP bandwidth when compared to traditional patch antennas of the same height. However, the obtained ARBW was 2.33% and structure complexity increased also. In [17], a novel stacked structure is proposed to enhance AR direction and CP bandwidth. The design is based on overlapping between the two CP regions to increase the ARBW. Therefore, the obtained simulation CP bandwidth is improved to 4.1%. Moreover, the design is used in MIMO design to accommodate the 5G requirement. In [18], a new wide ARBW CP antenna design is proposed. The authors depend on the study of resonant modes TM1/2,0, TM1/2,1, and TM3/2,0. They suppressed non-broadside modes. At the same time, the EMC around the patch is forced to be orthogonal and rotate sequentially. By this approach, the achieved ARBW is enhanced by 3.3 times compared to the traditional counterpart. In[19], single-feed and wideband CPMA is proposed for FRID applications. The antenna is bulky because it contains three stacked layers but it has a good ARBW which is equal to (13.4%). The author in this design used a circular slot etched on the lower patch in the diagonal axis to produce CP radiation. In[20], broadband CPMA is proposed based on capacitive coupling between the feeding network and driven patches. Each driven patch is coupled with two parasitic patches to produce additional CP modes. The parasitic elements increase antenna size if compared with other CP antenna operating at the same band. However, the design has an ARBW equal to 12.9% with a complicated feeding network. In [21], a stacked square ring dual bands antenna is proposed for CP generation. A parasitic open loop square ring is built over a driven patch to enhance ARBW. Good size reduction is obtained. Meanwhile, the CP bandwidth is equal to 1.2% which is too narrow. Authors in [22] proposed wide ARBW using rectangular strips as parasitic elements. conventional current truncating square patch antenna is surrounded by four rectangular strips. good ARBW is achieved compared to [19] which is equal to 24% but the antenna size seems to be larger. In [23], abroad band CP is designed for L-Band applications. The design depends upon a capacitive coupled feed network and parasitic ring slot to broaden ARBW. The achieved CP bandwidth was 16% at the centre frequency of 1593GHz. Unfortunately, the antenna has a complex profile. In [24], a compact size, dual-band CP antenna is simulated and fabricated. Two FR-4 substrates are stacked in order to obtain driven and parasitic patches. Driven patch is used to generate two degenerated orthogonal modes with equal amplitude and 90-degree phase difference. While, parasitic patch is used to generate the two bands of the axial ratio. Unfortunately, the antenna has narrow AR bandwidths, unstable gain over the interested bands, and absence of CP sense. In addition, the used cross slots techniques are not preferred in antenna design due to impedance matching area restrictions as illustrated in [5].

It can be understood from the above survey spot that most research focuses on developing a new antenna with compact size, wideband CP, acceptable broadside gain, and comparable radiation features. Among all the techniques used, CP bandwidth enhancement based on the parasitic effect is still a hot topic and an active research field. Therefore in this paper, a new single-feed and wideband circular polarization patch antenna based on parasitic effect is proposed for ISM band applications. The main contributions of the paper are:

1- A new wideband CP antenna with a simple structure and compact size is designed and fabricated for ISM band applications. Antenna size is equal to $0.451\lambda_o \times 0.451\lambda_o \times 0.026\lambda_o$ at central frequency 2.45GHz.
2- ARBW is enhanced by using novel patch geometry. The proposed geometry includes a peripheral cuts circular patch as a driven element, an inverted U-shape stub as a parasitic patch, and a proximity-coupled feeding line.
3- The idea behind the design proposes that every driven and parasitic patch would produce its own CP radiation. Therefore, the antenna's axial ratio bandwidth is expanded by creating two neighboring axial ratio (AR) minima points. That is, the increase in ARBW is up to 36% from that of the traditional circular patch antenna without parasitic effect. The proposed antenna has measured impedance bandwidth (IBW) of 8.5% and axial ratio bandwidth (ARBW) of 4.5% at a center frequency of 2.45GHz. In addition, the antenna exhibits a flat gain of 4.8 dB over the ISM band. This paper is

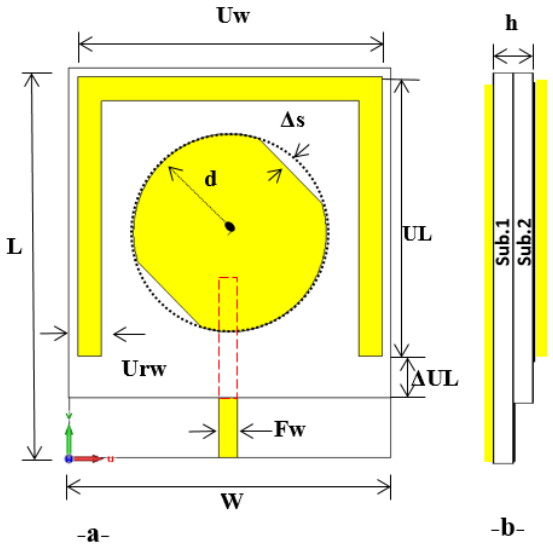

Figure. 1 Geometry of proposed Antenna: (a) Top view and (b) Side view

Table 1. Proposed antenna dimensions

Dim.	Value (mm)	Dim.	Value (mm)
L	65	UL	46
W	55	d	16.5
Uw	52	Fw	3.2
H	3.2	Urw	4
Δs	1.9	ΔUL	7

organized as follows. Antenna geometry and design methodology are reported in the next section. AR bandwidth enhancement analysis is discussed in section 3. Measured results and the comparison with other reported antennas are presented in section 4. A conclusion is finally, considered in section 5.

2. Antenna geometry and design methodology

Fig. 1 shows the geometry of the designed antenna. The antenna is designed to be symmetrical along the y-axis. Two 1.6 mm-thick FR-4 substrates with a dielectric constant $\varepsilon_r = 4.4$ and losses tangent $\delta = 0.002$ are stacked using special glue to increase substrate thickness (h). As a basic rule, the thick substrate contributes to bandwidth enhancement. The upper substrate consists of the microstrip circular patch as a driven patch surrounded by an inverted U-shape stub as a parasitic patch. To enable CP radiation, two peripheral cuts of depth (Δs) are made at the patch boundary diagonally. Besides, the lower substrate consists of a proximity-coupled feeding line and ground plane. In addition, two slits are made in the ground plane to increase matching conditions. The two substrates have the same width but different lengths due to feeding fabrication necessities.

To explain the design steps, three structures are made until reaching the final one as shown in Fig. 2. Also, the simulation results of the reflection coefficient and the Axial Ratio (AR) for each step of the structure are shown in Fig. 3. Ant.1 is the initial step. In this step, a microstrip circular patch antenna with a radius (d) is designed to work with a central frequency (f_r =2.45GHz) according to the standard formula given in Eq.(1). Simultaneously, the substrate width and length are calculated according to empirical Eq. (2) [25].

$$d = \frac{x}{[1+\frac{2h}{\pi\varepsilon_r x}[\ln(\frac{\pi x}{2h})+1.7726]]^{0.5}} \quad (1)$$

Where

$$x = \frac{8.791\times10^9}{f_r\sqrt{\varepsilon_r}}$$
$$L = W \cong 6h + r \quad (2)$$

In addition, substrate height (h) is increased by stacking two FR-4 substrates to enhance impedance bandwidth (|S11| < -10dB) and enabling proximity-coupled feeding line structure. This is because (Q_{rad}) is inversely proportional to the substrate height (h) for thin substrates ($h \ll wavelength$ (λ)). Therefore, increasing (h) will reduce (Q_t) and enhance impedance bandwidth according to Eq.(3) and Eq.(4) respectively [25].

$$\frac{1}{Q_t} = \frac{1}{Q_{rad}} \quad (3)$$

$$\frac{\Delta f}{f_o} = \frac{VSWR-1}{Q_t\sqrt{VSWR}} \quad (4)$$

Where, Q_t: total quality factor , Q_{rad} : quality factor due to radiation losses, ($\Delta f/f_o$): fractional band width (FBW), and VSWR: voltage standing wave ratio. The antenna in this step has one resonance frequency with linear polarization because the value of AR is larger than 3dB as shown in Fig. 3 (b). In the second step (Ant.2), two peripheral cuts are made at both opposite sides of the driven patch with (ΔS) depth as shown in Fig. 2. The details of this method can be found in [5, 26]. At this stage of design, the antenna has left-hand circular polarization (LHCP) radiation with a 3dB axial ratio (AR), and (ARBW) which are equal to 0.71dB and 1.9% respectively. The radiation at this stage has two degenerated and orthogonal electrical field components (modes) at the frequencies 2.38GHz and 2.45GHz as shown in

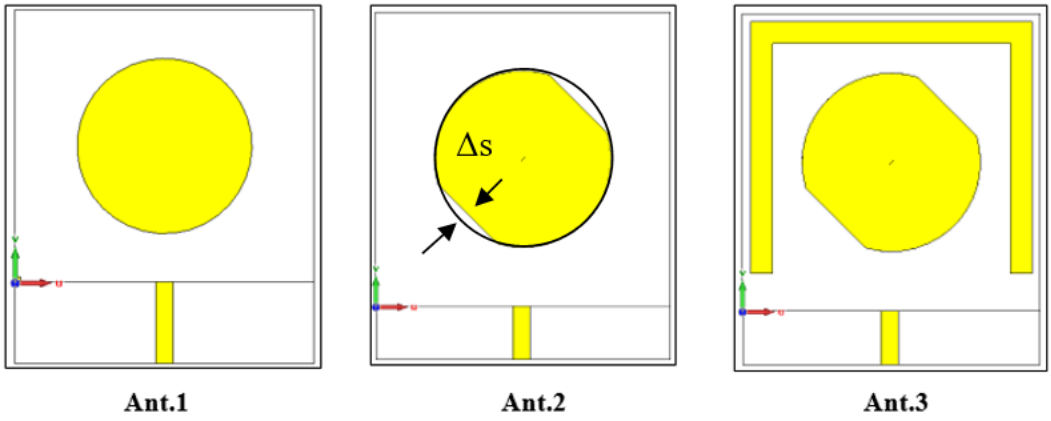

Figure. 2 Steps until reach to final antenna geometry

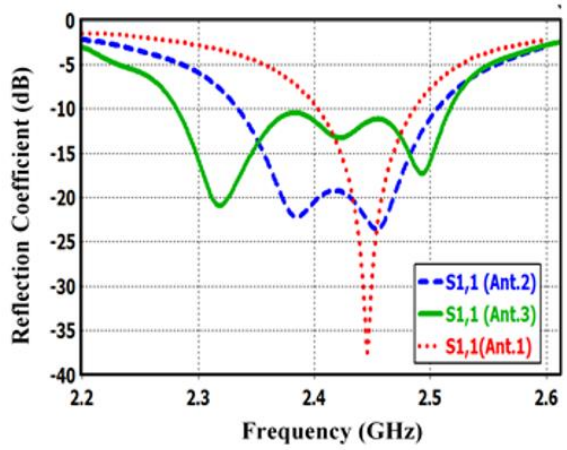

(a)

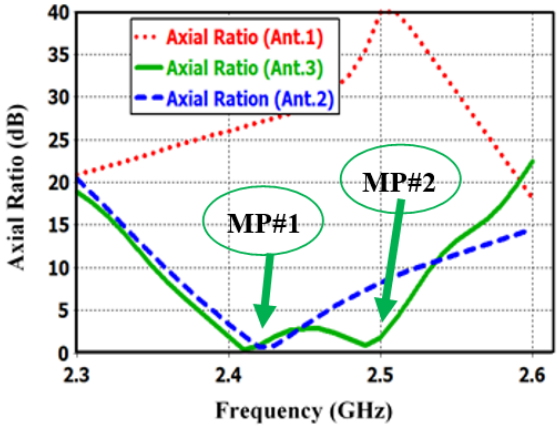

(b)

Figure. 3 CP parameters during antenna design: (a) Reflection Coefficient and (b) Axial ratio curves

Fig. 3 (a). These components have equal amplitude and a out of phase by 90° as will explained later. Theoretically, This behavior is subjected to Eq. (5) [25].

$$\boldsymbol{E_t(z;t) = E_x(z;t)\,\widehat{a_x} + E_y(z;t)\,\widehat{a_y}} \qquad (5)$$

Where: $E_t(z;t)$: total radiated electrical field in the z-direction (Propagation direction).

$E_x(z;t)$: radiated electrical field in the x-direction and equal to:

$$\boldsymbol{E_x(z;t) = E_{xo}\cos(\omega t + \phi_x)}$$

$E_y(z;t)$: radiated electrical field in the y-direction and equal to:

$$\boldsymbol{E_y(z;t) = E_{yo}\cos(\omega t + \phi_y)}$$

Where $\boldsymbol{E_{xo}}$ and $\boldsymbol{E_{yo}}$ represent Max. amplitude of the field components in the x and y direction respectively. Therefore, the AR value will be obtained by [25]:

$$\textbf{axial ratio (dB)} = \mathbf{20\log_{10}\left[\frac{E_{xo}}{E_{yo}}\right]} \qquad (6)$$

In the third step (Ant.3), Ant.2 is loaded by an inverted U-shape parasitic stub. This stub has equal-length arms and a fixed width overall the structure. The initial length of the stub before the optimization is estimated by Eq. (7) [25].

$$\boldsymbol{2UL + U_w = \frac{\lambda_g}{4} * 3} \qquad (7)$$

Where λ_g: guided wavelength. The coupling between the driving patch and the stub adds a new axial ratio point at the higher frequency region. At this stage, two adjacent AR minima points (MP) are generated as shown in Fig. 3 (b). These points make ARBW wider to approximately double. To this end, the obtained impedance bandwidth is equal to (10%) starting from (2.28GHz) to (2.517GHz). While the AR bandwidth is equal to (4.89%) starting from (2.39GHz) to (2.51GHz). The final optimized geometric parameters are listed in Table 1. CST full wave simulator software version 14.2 is used in the simulation and optimization.

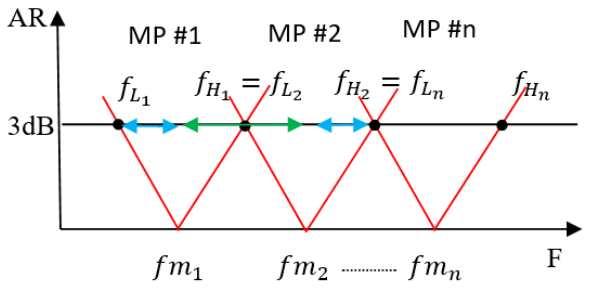

Figure. 4 Adjacent AR minima points (MP) and total bandwidth

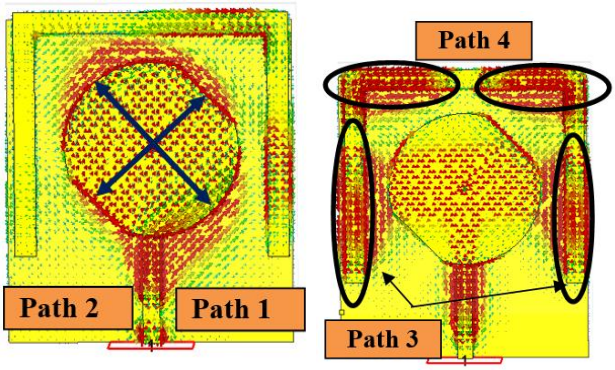

(a) (b)

Figure. 5 Surface current distributions: (a) Surface current paths at to driven patch (b) Surface current pathes at the parasitic patch

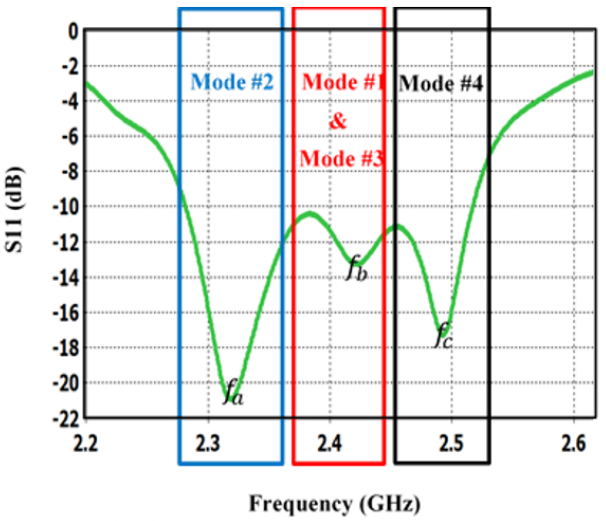

Figure. 6 Excited modes and its frequency regions

3. AR Bandwidth enhancement analysis

Two AR minima points (MP) are generated to achieve wider AR bandwidth ($\mathbf{BW_{Total}}$) . This proposed idea can be a proof mathematically for (n) AR minima points based on Fig. 4 and Eq.(8). That is, for maximum separation between any two adjacent AR Minima Points (MP), there is ($f_{H_{(n-1)}} = f_{L_n}$) at 3dB level. Therefore,

$$\mathbf{BW_{Total}} = (\mathbf{fm_1} - \mathbf{f_{L_1}}) + (\mathbf{fm_2} - \mathbf{f_{m_1}}) + (\mathbf{f_{H_2}} - \mathbf{f_{m_2}})$$
$$= (\mathbf{fm_1} - \mathbf{f_{L_1}}) + (\mathbf{f_{H_2}} - \mathbf{f_{m_2}}) + \Delta$$
$$= \frac{\mathbf{BW_1}}{2} + \frac{\mathbf{BW_2}}{2} + \Delta$$
$$\textit{for Ideal case } (\mathbf{BW_1} \cong \mathbf{BW_2} \cong \mathbf{BW_n})$$
$$\mathbf{BW_{Total}} = \mathbf{BW_1} + \mathbf{n} * \Delta \quad (8)$$

Where ($\mathrm{BW_n}$): bandwidths from each (MP #n) , (fm_n): frequency at MP occurred, (Δ): separation between two adjacent AR MP.

According to theory, CP is only possible when the total electric field comprises two components characterized by 1) Orthogonal, equal magnitudes. 2) a 90-degree phase difference between them [1].

For point 1, the orthogonality of the components for each AR can be achieved by creating two perpendicular surface current paths with a small length difference [17]. Therefore, in this design, four paths are designed to achieve two AR points. The first and second paths are obtained from the peripheral cuts at the boundary of the driven patch itself as shown in Fig. 5 (a). These paths are responsible for generating mode#2 and mode#1 at the frequencies ($f_a = 2.32GHz$) and ($f_b = 2.42$GHz) respectively as shown in Fig. 6. Meanwhile, the third and fourth paths are obtained by the inverted U-shape parasitic stub due to the null point located in each arm as shown in Figure (5-b). These paths produce modes #3 and #4 at ($f_b = 2.42$GHz) and ($f_c = 2.49$GHz) respectively as shown in Fig. 6. It is important to note here that the lengths of Path 3 and Path 1 are comparable (≈28mm) so that Mode #1 and Mode #3 are overlapped at the frequency ($f_b = 2.42$GHz). In addition, the magnitude of electrical field components (V/m) are approximately equal as shown in Fig. 7.

For point 2 and to show the differences in phase, screenshots for electrical field rotation are taken at a set time using CST software. It can be seen from Fig. 7 that the electric field associated with mode #1 is oriented at an angle of (+45°) with the x-axis. In contrast, the concentration of the electric field associated with mode #2 is oriented with the x-axis at a (– 45°) angle. As a result, the CP requirements have been met and the first AR minima point between these two modes is generated. In addition, mode #3 and mode #4 are orthogonally distributed along ±45° with the x-axis as seen in the same Figure. In this case, both mode #1 and mode#3 have the same orientations

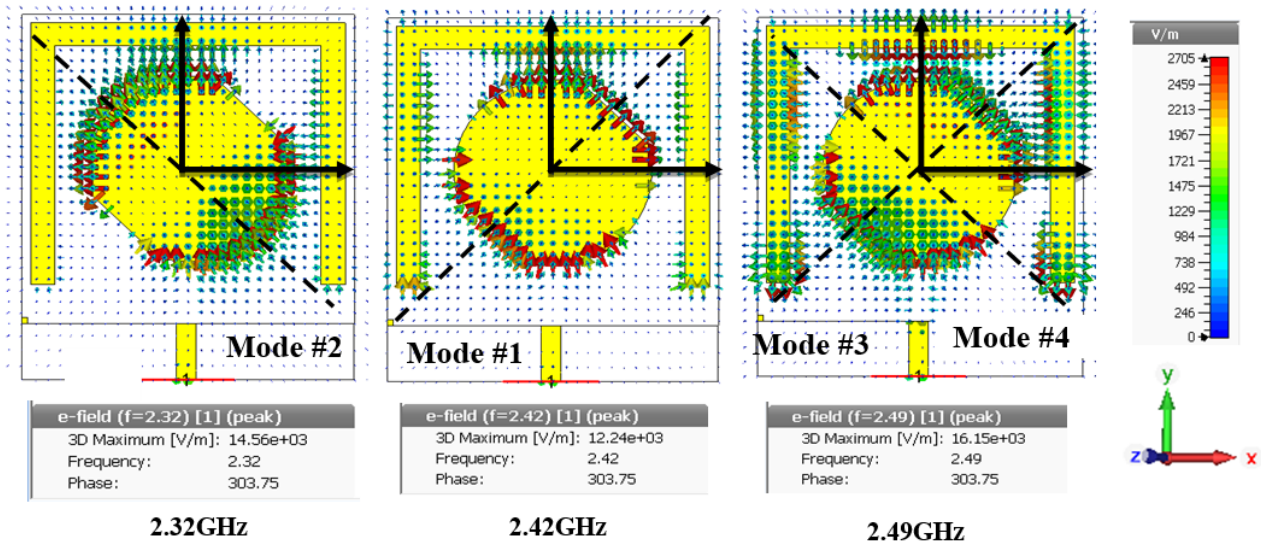

Figure. 7 Electric field distribution at the four resonant frequencies

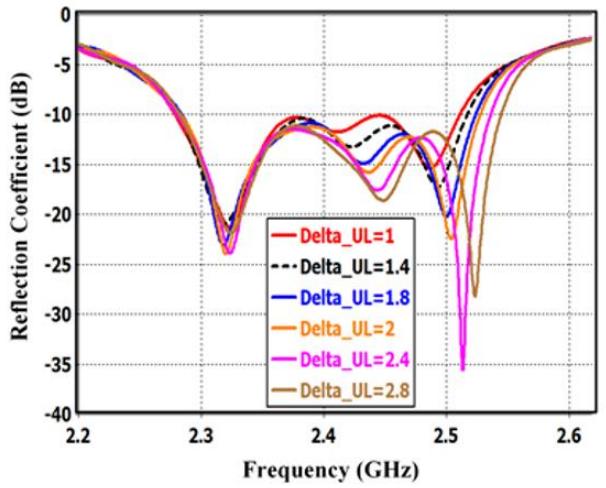

(a)

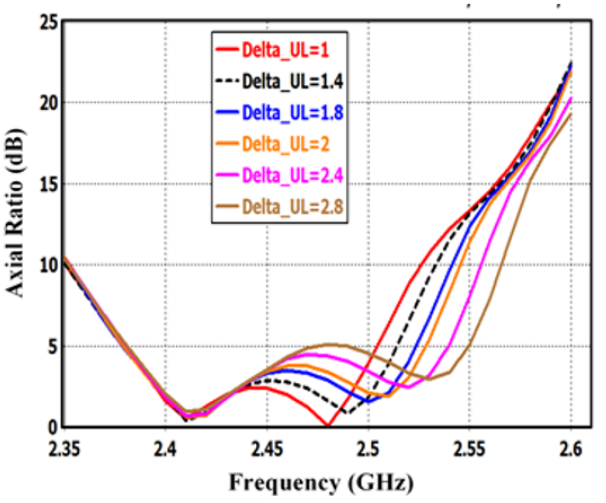

(b)

Figure. 8 Parametric study: (a) Effect of varying ΔUL on reflection coefficient and (b) AR of the proposed antenna

in (+45). As a result, CP conditions are met for the second time and a new minimum AR point is generated between mode #3 and mode #4. Therefore, the two adjacent AR points increase AR bandwidth.

To verify the above analysis of the antenna's operation, key geometrical parameters are parametrically studied here. It should be noted that the studies were carried out by changing one parameter at a time, with other parameters being fixed as mentioned in Table 1. According to Fig. 8, it is found that the (ΔUL) parameter has a significant impact on both $|S11|$ and AR responses. This is because the parasitic stub mainly generates the third and fourth modes. Therefore, the length of parasitic arms has a significant effect in determining the position of the mode's resonant frequency. decreasing arm length pushes the resonant modes to a higher frequency while increasing it has the opposite effect.

Consequently, the second minimum point of AR will shift to a higher frequency region until vanishes. Additionally, it observed that the first and second modes with the first AR point were not affected by changing (ΔUL). As a final result of this study, the optimized (ΔUL) length is selected to be 1.4mm which covers the ISM band. On the other hand, Fig. 9 shows the outcomes results of $|S11|$ and AR according to change in (Δs). As anticipated, the depth of the peripheral cuts (Δs) in the patch boundary directly impacts the degenerated modes #1 and #2, and consequently, CP bandwidth. Initially (Δs) set to (1.3mm), one dominant mode is generated as seen in the same figure. However, when (Δs) increased to (1.5mm), modes #1 and #2 appeared and they had equal amplitude and 90° phase difference which led

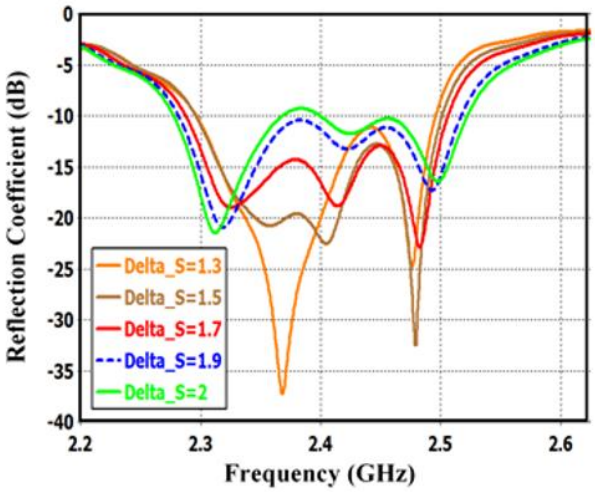

(a)

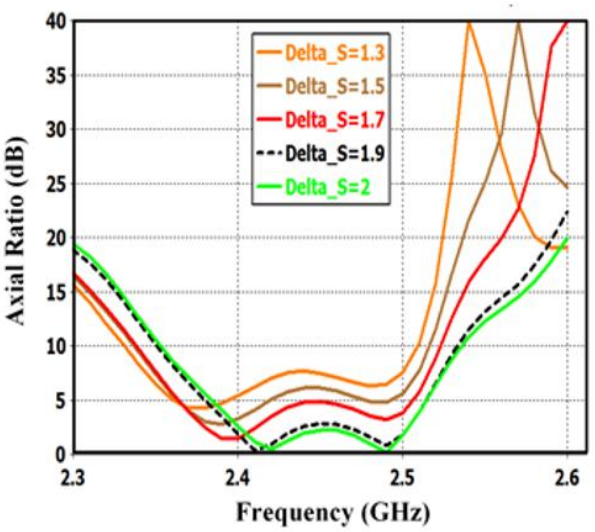

(b)

Figure. 9 Parametric study , effect of varying (Δs) on: (a) S11 and (b) AR

to making the first AR minimum point. Therefore, (Δs) controls the left region of AR bandwidth. The best value is found to be 1.9mm.

4. Experimental results and discussion

Fig. 10 shows photographs of the fabricated antenna and its measurement setup. The practical experiments are performed in an anechoic chamber and MS4642A vector network analyzer is used in the measurements. Meanwhile, CST Microwave Studio Simulation Suite software is used for fine-tuning and optimization during the simulations. In general, good matching is achieved between the simulation and measured results with reasonable deviations due to fabrication and measurement errors. Fig. 11 illustrates the simulation and measured curves of the reflection coefficients |S11|. It can be seen that the

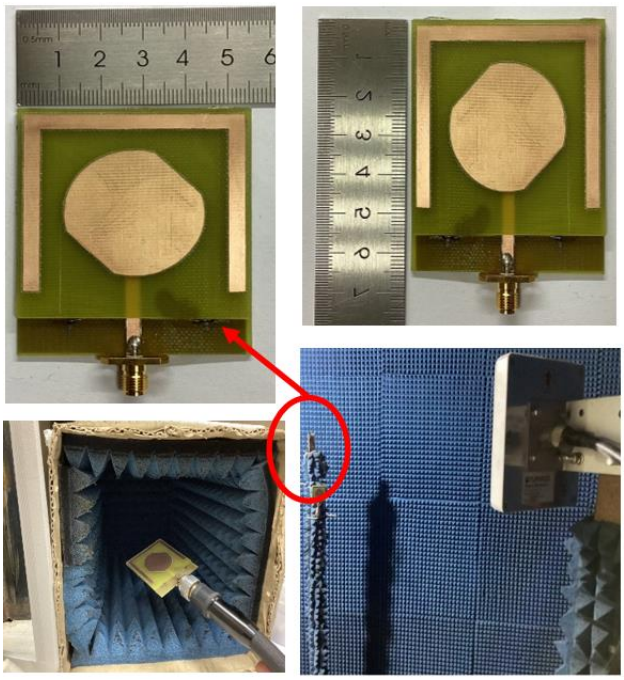

Figure. 10 Photograph and measurement setup of the designed antenna

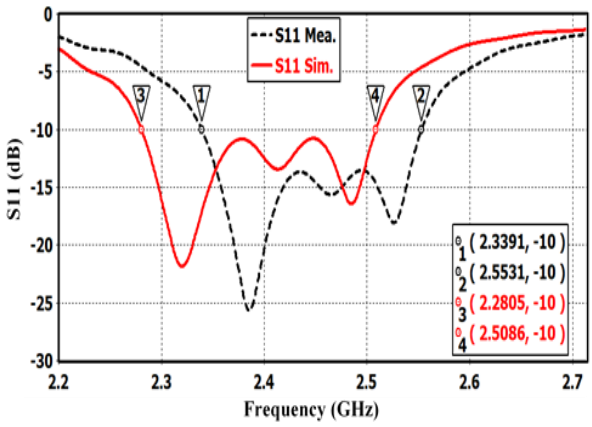

Figure. 11 Simulated and measured reflection coefficients of the proposed antenna

antenna has three resonant frequencies at (2.32GHz),(2.42GHz), and (2.49GHz). The achieved simulated |S11| < -10 bandwidth is around (10%) starting from (2.28GHz) to (2.517GHz). While the measured one is around (8.5%), starting from (2.33GHz) to (2.55GHz).

The shift between the two results may come from the air gaps that still exist between the two substrates after the fabrication and due to misalignment. Fig. 12 shows circular polarization results, the designed antenna exhibits LHCP sense in the required frequency band. Moreover, the obtained minimum values of AR are around (0.56dB) in both simulation and measurement at (2.41GHz), and (2.44GHz) frequencies respectively. The simulated axial ratio

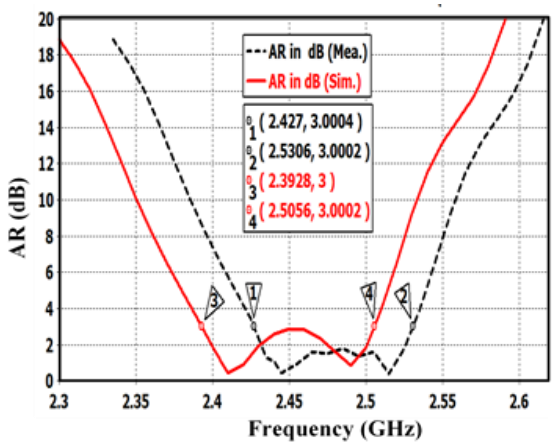

Figure. 12 Simulated and measured axial ratio

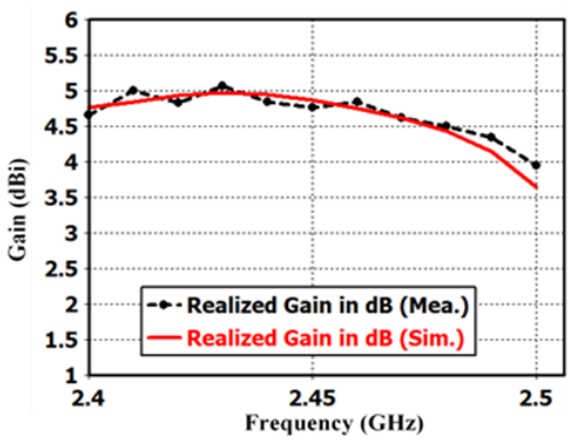

Figure. 13 Simulated and measured of realized gain for the proposed antenna

bandwidth (AR < 3dB) is equal to (4.89%) starting from (2.39GHz) to (2.51GHz) while the measured one is equal to (4.5%) starting from (2.42GHz) to (2.53GHz). In addition, Fig. 13 shows the antenna's realized gain in the broadside direction. Approximately flat gain of around 4.8dB over the entire band of interest for both simulation and measured results. Fig. 14 depicts the simulated and measured results of radiation patterns. Both the X-Z plane and Y-Z plane are plotted at three different frequencies. For all the selected frequencies, the worst co-pol / x-pol ratio is better than 13dB in the antenna broadside direction which indicates acceptable polarization purity.

The designed antenna has comparable features. To show the advantages of the proposed antenna over other related near works, a comparison study is made with the traditional CP circular patch antenna and some existing important works in the literature as seen in Table 2. It is obvious that the designed antenna is characterized by:

1- Compact size and low manufacturing complexity compared to the reported antennas. The designed antenna has better size reduction which is obtained by using high dielectric constant material in the substrates. In addition, stacking two substrates increases (h) which reduces the driven patch radius as illustrated in Eq.(1)
2- The proposed antenna processes better impedance and wider AR bandwidths with an excellent overlap. This point represents the main contribution of the article. For the Impedance bandwidth (IBW), the three adjacent resonance modes at different frequencies are combined to produce the wide (IBW) as shown in Fig. 11. Since a proximity-feeding line is used, good impedance matching is achieved over the desired band. In the same context, increasing (h) by stacking two substrates improves the bandwidth as mentioned in Eq. (3) and Eq. (4). The measured IBW is around (8.5%), starting from (2.33GHz) to (2.55GHz) which covers the entire ISM band frequencies. For the Axial Ratio Bandwidth (ARBW), the driven and parasitic patches produced an adjacent pair of degenerated and orthogonal modes with 90 degrees out of phase. Therefore, the obtained ARBW represents the algebraic addition of the two bandwidths.Therfore increasing by 36% is obtained. The measured ARBW is equal to (4.5%) starting from (2.42GHz) to (2.53GHz).
3- The antenna has better realized gain value over the band of interest. This is due to the symmetric geometry along the y-z plane and the complete ground plane beneath the patches.
4- Therefore, and for all of the above, the designed antenna can be a candidate to operate for ISM applications.

5. Conclusion

In this paper, a new and compact CP antenna is successfully designed and fabricated for ISM band applications. The novel geometry of the antenna generates four resonant modes which produce two adjacent AR points. The first and second modes are achieved by truncating the main driven patch while the third and the fourth modes are achieved by the parasitic element surrounding the main patch. Consequently, AR bandwidth is enhanced greatly as shown previously in Table 2. The proposed antenna has measured IBW of 8.5% and ARBW of 4.5% at a center frequency of 2.45GHz. In addition, the antenna exhibits a flat gain of 4.8 dB over the ISM band. A

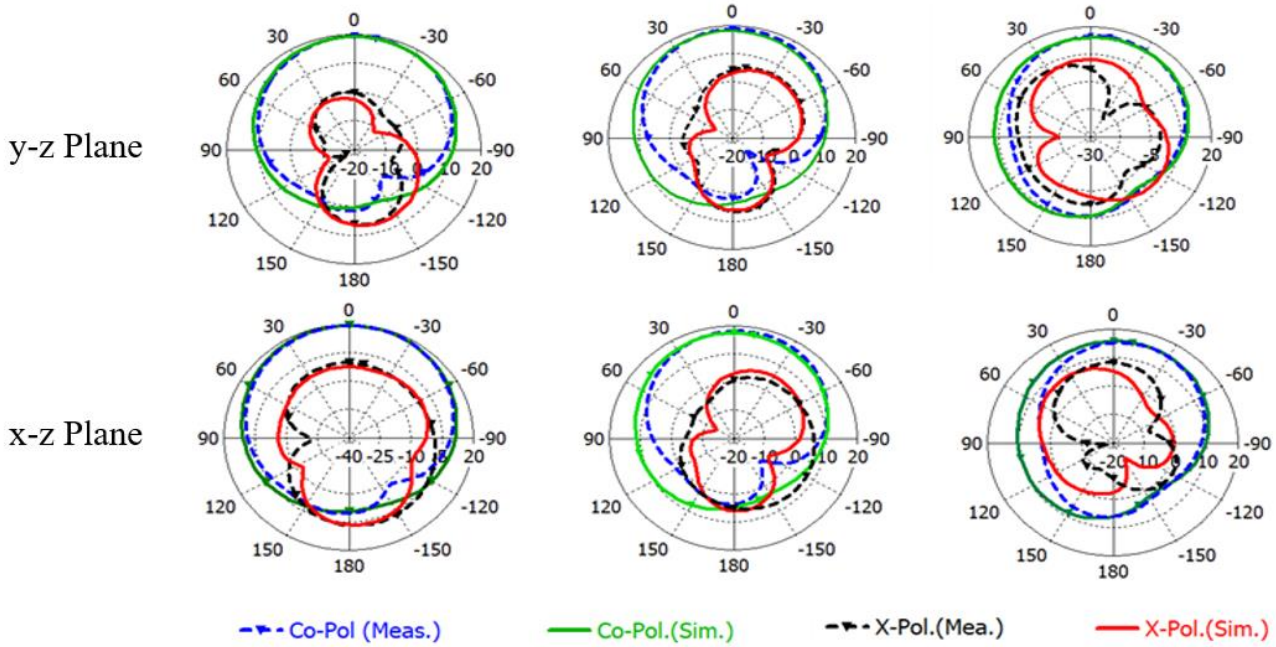

Figure. 14 Simulated and measured radiation patterns of the proposed antenna

Table 2. Comparison of the proposed antenna with different related works

Ref.	Dimensions $\times (\lambda^o)^3$	IBW	ARBW	Real. Gain (dB)	Number of Layers
Traditional (Ant.2)	$0.4 \times 0.43 \times 0.026$	7%	1.6%	5	2
[14]	$0.68 \times 0.68 \times 0.044$	6.6%	3.85%	7.2	3
[15]	$0.5 \times 0.27 \times 0.016$	6%	3.3%	2.7	1
[16]	$0.5 \times 0.27 \times 0.016$	4.6%	2.33%	--	2
[17]	$\cong 0.34 \times 0.34 \times 0.004$	10.8%	4.1%	3	2
[18]	$0.58 \times 0.56 \times 0.03$	5.4%	5%	4.5	2
[19]	$0.601 \times 0.601 \times 0.8.95$	21%	13.4%	7	3
[21]	N/A	3.95%	1.2%	3.7	2
[24]	N/A	≈ 1.05%	Max.=1.4%	≈ 3.8	2
Prop.	$\mathbf{0.451 \times 0.451 \times 0.026}$	**8.5%**	**4.5%**	**4.8**	**2**

small expected shift between the simulated and measured results is obtained due to fabrication tolerances. In the future, authors will use the proposed antenna in the MIMO system for WLAN applications.

Conflicts of interest

"The authors declare no conflict of interest"

Author contributions

"Conceptualization, Alaa I. Al-Muttairi; methodology, Alaa I. Al-Muttairi; software, Alaa I. Al-Muttairi; validation, Mohammed J. M. Ameen, and Ali Khalid Jassim; formal analysis, Alaa I. Al-Muttairi; investigation, Alaa I. Al-Muttairi; resources, Alaa I. Al-Muttairi; writing—original draft preparation, Alaa I. Al-Muttairi; writing—review and editing, Alaa I. Al-Muttairi; visualization, Mohammed J. M.; supervision, Ali Khalid Jassim; project administration, Alaa I. Al-Muttairi; funding acquisition, Alaa I. Al-Muttairi", etc. Authorship must be limited to those who have contributed substantially to the work reported.

Acknowledgments

The authors would like to thank the University of Babylon / Babylon-Iraq and Mustansiriyah University / Baghdad-Iraq for their support in the present work.

References

[1] S. S. Gao, Q. Luo, and F. Zhu, *Circularly polarized antennas*, John Wiley & Sons, UK, Vol. 1, 2014.

[2] N. Hussain, T. D. Pham, and H. H. Tran, "Circularly polarized MIMO antenna with wideband and high isolation characteristics for C-band communication systems", *Micromachines*, Vol. 13, No. 11, p. 1894, 2022.

[3] H. D. Chen and W. S. Chen, "Probe-fed compact circular microstrip antenna for circular polarization", *Microwave and Optical Technology Letters*, Vol. 29, No. 1, pp. 52-54, 2001.

[4] J. R. James and P. S. Hall, *Handbook of microstrip antennas*, IET, UK, Vol. 1,1989.

[5] W. S. Chen, "Small circularly polarized microstrip antennas", In: *Proc. of IEEE Antennas and Propagation Society International Symposium. 1999 Digest. Held in conjunction with: USNC/URSI National Radio Science Meeting (Cat. No. 99CH37010)*, Vol. 1, pp. 256-259, 1999.

[6] K. M. Mak, H. W. Lai, K. M. Luk, and K. L. Ho, "Polarization reconfigurable circular patch antenna with a C-shaped", *IEEE Transactions on Antennas and Propagation*, Vol. 65, No. 3, pp. 1388-1392, 2016.

[7] X. Qing and Z. N. Chen, "Compact asymmetric-slit microstrip antennas for circular polarization", *IEEE Transactions on Antennas and Propagation*, Vol. 59, No. 1, pp. 285-288, 2010.

[8] F. Yang and Y. R. Samii, "A reconfigurable patch antenna using switchable slots for circular polarization diversity", *IEEE Microwave and Wireless Components Letters*, Vol. 12, No. 3, pp. 96-98, 2002.

[9] M. Haneishi and S. Yoshida, "A design method of circularly polarized rectangular microstrip antenna by one-point feed", *Electronics and Communications in Japan (Part I: Communications)*, Vol. 64, No. 4, pp. 46-54, 1981.

[10] K. U. Sam and P. Abdulla, "Truncated circular microstrip ultra wideband antenna exhibiting wideband circular polarization", *Progress in Electromagnetics Research C*, Vol. 99, pp. 111-122, 2020.

[11] W. S. Chen, C. K. Wu, and K. L. Wong, "Single-feed square-ring microstrip antenna with truncated corners for compact circular polarisation operation", *Electronics Letters*, Vol. 34, No. 11, pp. 1045-1046, 1998.

[12] A. K. Bhattacharyya and L. Shafai, "A wider band microstrip antenna for circular polarization", *IEEE Transactions on Antennas and Propagation*, Vol. 36, No. 2, pp. 157-163, 1988.

[13] J. H. Lu and K. L. Wong, "Single-feed circularly polarized equilateral-triangular microstrip antenna with a tuning stub", *IEEE Transactions on Antennas and Propagation*, Vol. 48, No. 12, pp. 1869-1872, 2000.

[14] H. C. Yang, X. Y. Liu, Y. Fan, and M. M. Tentzeris, "Flexible circularly polarized antenna with axial ratio bandwidth enhancement for off-body communications", *IET Microwaves, Antennas & Propagation*, Vol. 15, No. 7, pp. 754-767, 2021.

[15] J. F. Lin and Q. X. Chu, "Enhancing bandwidth of CP microstrip antenna by using parasitic patches in annular sector shapes to control electric field components", *IEEE Antennas and Wireless Propagation Letters*, Vol. 17, No. 5, pp. 924-927, 2018.

[16] M. C. Tang, X. Chen, M. Li, and R. W. Ziolkowski, "A bandwidth-enhanced, compact, single-feed, low-profile, multilayered, circularly polarized patch antenna", *IEEE Antennas and Wireless Propagation Letters*, Vol. 16, pp. 2258-2261, 2017.

[17] F. M. Alnahwi, Y. I. A. Yasir, C. H. See, and R. A. A. Alhameed, "Single-element and MIMO circularly polarized microstrip antennas with negligible back radiation for 5G mid-band handsets", *Sensors*, Vol. 22, No. 8, p. 3067, 2022.

[18] N. W. Liu, L. Zhu, Z. X. Liu, G. Fu, and Y. Liu, "Design approach of a single circularly polarized patch antenna with enhanced AR-bandwidth under triple-mode resonance", *IEEE Transactions on Antennas and Propagation*, Vol. 68, No. 8, pp. 5827-5834, 2020.

[19] X. Qing and Z. N. Chen, "A wideband circularly polarized stacked slotted microstrip patch antenna", *IEEE Antennas and Propagation Magazine*, Vol. 55, No. 6, pp. 84-99, 2013.

[20] K. Ding, C. Gao, D. Qu, and Q. Yin, "Compact broadband circularly polarized antenna with parasitic patches", *IEEE Transactions on Antennas and Propagation*, Vol. 65, No. 9, pp. 4854-4857, 2017.

[21] D. Seo and Y. Sung, "Stacked open-loop square ring antenna for circular polarization operation", *IEEE Antennas and Wireless Propagation Letters*, Vol. 14, pp. 835-838, 2014.

[22] J. Wu, Y. Yin, Z. Wang, and R. Lian, "Broadband circularly polarized patch antenna with parasitic strips", *IEEE Antennas and*

Wireless Propagation Letters, Vol. 14, pp. 559-562, 2014.

[23] S. Fu, Q. Kong, S. Fang, and Z. Wang, "Broadband circularly polarized microstrip antenna with coplanar parasitic ring slot patch for L-band satellite system application", *IEEE Antennas and Wireless Propagation Letters*, Vol. 13, pp. 943-946, 2014.

[24] S. Kumar, B. K. Kanaujia, M. K. Khandelwal, and A. Gautam, "Stacked dual-band circularly polarized microstrip antenna with small frequency ratio", *Microwave and Optical Technology Letters*, Vol. 56, No. 8, pp. 1933-1937, 2014.

[25] C. A. Balanis, *Antenna theory: analysis and design*, John Wiley & Sons, USA, Vol. 4 , 2016.

[26] W. S. Chen, C. K. Wu, and K. L. Wong, "Compact circularly-polarised circular microstrip antenna with cross-slot and peripheral cuts", *Electronics Letters*, Vol. 34, No. 11, pp. 1040-1040, 1998.